https://doi.org/10.5194/egusphere-2026-2580
Preprint. Discussion started: 13 May 2026

Orbital-scale hydroclimate variations in the western Qaidam Basin during the Late Pliocene: evidence from magnetic parameters and median grain size

Zeng Luo[1*], Hansheng Wang[1,2], Xiaoli Yu[1], Zhongbao Zhang[3], Zhifen Song[1], Jing Yang[1], Wanfeng Chen[1], Qingda Su[4*], Yang Lu[5], Shun Hua[1]

[1]College of Geography and Tourism, Hunan University of Arts and Science, Changde, Hunan, China 415000.

[2]Key Laboratory of Western China's Environmental System (Ministry of Education), College of Earth and Environmental Sciences, Lanzhou University, Lanzhou, Gansu, China 730000

[3]College of Urban and Environmental Sciences, Hubei Normal University, Huangshi, Hubei, China 435002.

[4]Shandong Provincial Key Laboratory of Water and Soil Conservation and Environmental Protection, College of Resources and Environment, Linyi University, Linyi, Shandong, China 276000.

[5]Meteorological Bureau of Shunde District, Foshan, Guangdong, China 528399.

*Correspondence to: Zeng Luo (luozeng2020@foxmail.com); Qingda Su (suqingda@foxmail.com).

https://doi.org/10.5194/egusphere-2026-2580
Preprint. Discussion started: 13 May 2026

Abstract

A recent study suggests that the precipitation records of the Qaidam Basin during the middle Piacenzian warm period (mPWP, 3.264-3.025 Ma) are broadly consistent with those of the monsoon influenced regions, and are highly sensitive to 20-kyr precessional cycles, implying that the East Asian summer monsoon (EASM) intensified and migrated westward into the Asian interior during this warm interval. However, it remains unclear whether such a precession-dominated pattern persisted throughout the Late Pliocene or was restricted to specific intervals. To address this question, we present new magnetic parameter and median grain size records from the Gansen (GS) section for 3.6-3.25 Ma and 2.95-1.8 Ma, and integrate them with the previously published records for 3.25-2.95 Ma to assess orbital-scale precipitation variations in the western Qaidam Basin during the Late Pliocene. The results show that EASM-related summer moisture reached the western Qaidam Basin during 3.6-3.25 Ma, although the associated precipitation was weaker than during 3.25-2.95 Ma. Spectral analysis further reveals that precipitation variations during 3.6-3.3 Ma were characterized by dominant 100-kyr cyclicity rather than the previously reported precession-dominated pattern during 3.25-2.95 Ma, suggesting a nonlinear response to insolation forcing. This contrast indicates that the precession-dominated pattern was not a persistent feature throughout the Late Pliocene in the western Qaidam Basin. Instead, our results suggest that under different climatic background states, the dominant processes controlling the westward penetration of summer moisture into the western Qaidam Basin were also different, and that the 20-kyr and 100-kyr

https://doi.org/10.5194/egusphere-2026-2580
Preprint. Discussion started: 13 May 2026

periodicities mainly reflect these differences in forcing response. In addition, the similar phase variations between these precipitation records and the benthic oxygen isotope stack at the 40-kyr band imply that Antarctic ice sheets may have modulated hydroclimatic variations in the basin. These findings provide new insight into how background climate conditions may shape the orbital-scale response of precipitation, and more broadly hydroclimatic variations, in the Asian interior during warm periods.

Keywords: Late Pliocene; Qaidam Basin; Monsoon precipitation; Insolation forcing; Orbital cycles.

https://doi.org/10.5194/egusphere-2026-2580
Preprint. Discussion started: 13 May 2026

1 Introduction

With continued global warming, knowledge of climate variations during past warm periods has major implications for understanding future climate change. The middle Piacenzian warm period (mPWP: 3.264-3.025 Ma), a particularly well-documented warm interval during the Late Pliocene, has long been considered an ideal geological analog for interpreting the path of future anthropogenic warming (Ravelo et al., 2004; Raymo et al., 2006; Dowsett et al., 2010; Salzmann et al., 2011; Haywood et al., 2011; Lunt et al., 2012; Burke et al., 2018; Su et al., 2024; Luo et al., 2021, 2024; Zhou and Liu, 2025). Compared to the present, this interval was characterized by similar orbital configurations and geographic boundary conditions (Haywood et al., 2011; Su et al., 2024), higher atmospheric carbon dioxide concentrations (400-450 ppmv) (Bartoli et al., 2011; Badger et al., 2013; Haywood et al., 2016), small Arctic ice sheets (Brigham-Grette et al., 2013; Rahaman et al., 2020), elevated global temperatures (Burke et al., 2018), and increased sea levels (Hearty et al., 2020). Over the past two decades, numerous studies based on proxy reconstructions from loess deposits, lake sediments, and marine sediments, together with climate model simulations, have suggested that the mid-Piacenzian world was not only warmer but also wetter on most continents than today (Reguero et al., 2007; Salzmann et al., 2008, 2011; Brigham-Grette et al., 2013; Herbert et al., 2016; Yang et al., 2018; Vieira et al., 2018; Zhou and Liu, 2025). Similarly, in the Asian interior, the extent of arid regions decreased during the mPWP. For example, arid conditions in the Qaidam Basin, an important part of the Asian interior, were alleviated during the

https://doi.org/10.5194/egusphere-2026-2580
Preprint. Discussion started: 13 May 2026

mPWP, contributing to a regional contraction of the inland arid zone (Koutsodendris et al., 2019; Huang et al, 2019; Schwarz et al., 2022; Su et al., 2024). This occurred because the East Asian summer monsoon (EASM) migrated westward toward the western Qaidam Basin, bringing relatively more water vapor to this area and changing the local moisture conditions (Huang et al., 2019, 2021; Schwarz et al., 2022).

At the orbital timescale, recent precipitation records from the Gansen (GS) section of the western Qaidam Basin reveal dominant 20-kyr precessional cycles (Luo et al., 2024). These cycles are consistent with records from the Chinese Loess Plateau and the South China Sea (Wehausen and Brumsack, 2002; Wan et al., 2010; Luo et al., 2021), further indicating that the EASM strongly influenced precipitation in the Qaidam Basin during this warm interval. However, EASM influence on precipitation in the Qaidam Basin has also been inferred for other intervals of the Late Pliocene. For example, pollen records from the SG-1b core in the western Qaidam Basin show that annual mean precipitation during 3.5-3.0 Ma was about ten times higher than today and was associated with EASM (Koutsodendris et al., 2019; Schwarz et al., 2022). In addition, hematite-content records from the HTG section suggest that the EASM also affected precipitation variations in this region during the Late Pliocene (Su et al., 2024). These studies imply that EASM-related moisture may also have influenced precipitation during other Late Pliocene intervals, but whether this was accompanied by persistent precession-dominated cyclicity remains unresolved. Owing to the lack of high-resolution and continuous precipitation records, it is still unclear whether precession-dominated cyclicity was restricted to the mPWP or persisted

https://doi.org/10.5194/egusphere-2026-2580
Preprint. Discussion started: 13 May 2026

throughout the Late Pliocene, which limits our understanding of precipitation variations in the Asian interior during the Pliocene warmth. Existing studies have also reached different conclusions regarding the dominant orbital periodicity of Late Pliocene precipitation in the Qaidam Basin. For example, Su et al. (2024) proposed that precipitation variations were dominated by 40-kyr obliquity cyclicity, whereas Schwarz et al. (2022) argued for dominant 100-kyr eccentricity cyclicity. This discrepancy highlights the need for additional high-resolution records to determine whether precession-dominated precipitation variability was persistent throughout the Late Pliocene or restricted to specific warm intervals such as the mPWP.

To determine whether the precession-dominated precipitation pattern previously identified during 3.25-2.95 Ma was restricted to that interval or persisted through other stages of the Late Pliocene, we present new magnetic-parameter and median grain size records from the GS section in the Qaidam Basin for 3.6-3.25 Ma and 2.95-1.8 Ma. By integrating these new data with the previously published records for 3.25-2.95 Ma, we construct a longer precipitation record spanning 3.6-1.8 Ma and examine how orbital-scale precipitation variations in the western Qaidam Basin varied across different Late Pliocene intervals.

2 Geologic setting

The Qaidam Basin is located in the northeastern part of the Qinghai-Tibet Plateau, extending approximately from 35.9° to 39.3°N and from 90.3° to 99.3°E (Fig. 1). It is surrounded by several mountain ranges, including the Kunlun Mountains to the south, the Altyn Tagh Mountains to the northwest, the Qilian Mountains to the

https://doi.org/10.5194/egusphere-2026-2580
Preprint. Discussion started: 13 May 2026

133 northeast, and the Ela Mountains to the east (Fig. 1b). This mountain-surrounding
134 geographical pattern renders the Qaidam Basin relatively enclosed, forming a unique
135 climate and ecological environment. Because the basin is far from major moisture
136 source and lies in the rain shadow of the Tibetan Plateau, mean annual precipitation is
137 very low, ranging from only 50 to 200 mm, whereas mean annual evaporation is as
138 high as ~3000 mm (Cai et al., 2012; Wang et al., 2013; Yang et al., 2020; Luo et al.,
139 2024). As a result, the Qaidam Basin is characterized by a hyper-arid climate, with
140 widespread deposition of evaporite minerals such as halite, carbonates, and gypsum
141 (Li et al., 2010; Wang et al., 2013; Luo et al., 2018, 2024).

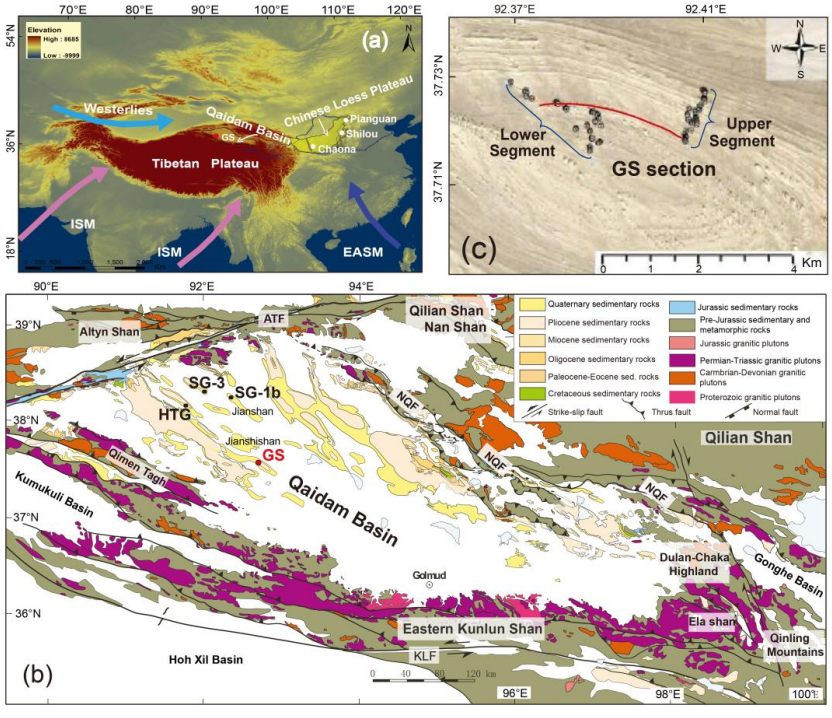

142

143 **Figure 1.** Locations of the study GS site. (a) The modern summer atmospheric
144 circulation pattern of Asia and the location of the GS section labeled with a red spot.

https://doi.org/10.5194/egusphere-2026-2580
Preprint. Discussion started: 13 May 2026

145 ISM: Indian summer monsoon. EASM: East Asian summer monsoon. (b) Detailed
146 geological map of the Qaidam Basin and the location of the GS section in the Qaidam
147 Basin. ATF: Altyn Tagh fault, KLF: Kunlun fault, NQF: North Qaidam fault. This
148 figure is modified after Bush et al. (2016). (c) A closer look at the GS section with a
149 satellite image showing the sample locations and their distribution between the lower
150 segment (0-226 m in stratigraphic height) and the upper segment (201-478 m in
151 stratigraphic height) of the stratigraphic section.

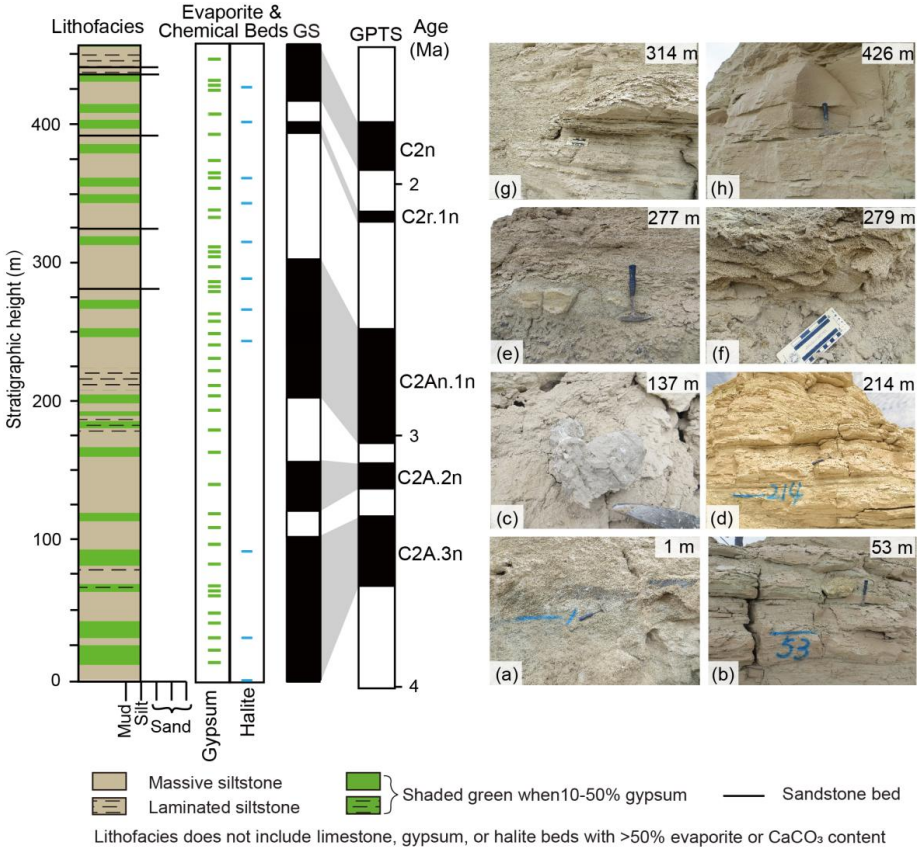

152

153 **Figure 2.** Lithology, age model and representative sediments in the GS section.

154 The studied GS section (37.717°N, 92.38°E to 37.73°N, 92.41°E) lies on the

https://doi.org/10.5194/egusphere-2026-2580
Preprint. Discussion started: 13 May 2026

southern flank of the anticline which is close to Jianshi Shan on the northwestern margin of the Qaidam Basin (Fig. 1b). Owing to the presence of thick salt and weathering crusts in the upper part of the section, only the lower 478 m was sampled. However, because the GS section is a composite stratigraphic succession composed of lower and upper segments that overlap between 201 and 226 m, the effective stratigraphic thickness is 453 m (Fig. 1c). The strata consist mainly of massive and laminated siltstone, interbedded with gypsum-rich siltstone and occasional sandstone beds (Fig. 2). Gypsum layers occur throughout the sequence, whereas halite layers are confined to the intervals between 0 and 105 m and between 262 and 453 m (Fig. 2). Previous paleomagnetic analyses indicate that the sampled 0-453 m interval of the GS section spans ~3.6-1.8 Ma (Luo et al., 2024).

3 Materials and methods

The chronology of the GS section is based on the previously published paleomagnetic framework (Luo et al., 2024), in which the observed polarity sequence was correlated with the geomagnetic polarity time scale, indicating that the sampled 0-453 m interval spans ~3.6-1.8 Ma. This age model provides the basis for plotting the new paleoclimatic records and conducting subsequent spectral analyses.

For magnetic analyses, low-frequency and high-frequency magnetic susceptibility (χ) of the 149 samples was measured at 976 Hz and 15616 Hz, respectively, using the AGICO multifunction spinner Kappabridge (MFK1-FA). frequency-dependent magnetic susceptibility (χ_{fd}) was calculated as $\chi_{fd}=\chi_{976Hz}-\chi_{15616Hz}$. Isothermal remanent magnetization (IRM) was then acquired in applied fields of 1.2 T

https://doi.org/10.5194/egusphere-2026-2580
Preprint. Discussion started: 13 May 2026

and -0.3 T, respectively. Hard isothermal remanent magnetization (HIRM) was subsequently calculated as $(IRM_{1.2T}+IRM_{-0.3T})/2$. Finally, the χ_{fd}/HIRM (the ratio of the frequency-dependent magnetic susceptibility to the intensity of the isothermal remanent magnetization) values of the 149 samples were calculated. All magnetic measurements were carried out at the Paleomagnetism Laboratory of the China University of Geosciences, Beijing, China.

For grain-size analysis, all 149 samples were pretreated before measurement. Approximately 0.3 g of each bulk sample was first treated with 10 mL of 30% H_2O_2 to remove organic matter and then with 10 mL of 10% HCl to remove carbonates. The samples were subsequently immersed in distilled water for 12 h. After removal of the supernatant, the samples were ultrasonically dispersed in 10 mL of 10% $(NaPO_3)_6$ solution for 10 minutes. Grain-size distributions were then measured using a Malvern Mastersizer 2000 laser grain-size analyzer. These measurements were conducted at the Key Laboratory of Western China's Environmental Systems, Lanzhou University.

4 Results

Because the χ_{fd}/HIRM and median grain size records for 3.25-2.95 Ma have been published previously (Luo et al., 2024), the present study focuses on the newly generated data for 3.6-3.25 Ma and 2.95-1.8 Ma and combines them with the published record for comparison. The reconstructed χ_{fd}/HIRM and median grain size records for 3.6-3.25 Ma and 2.95-1.8 Ma, together with the previously published records for 3.25-2.95 Ma (Luo et al., 2024), are shown in Fig 3.

https://doi.org/10.5194/egusphere-2026-2580
Preprint. Discussion started: 13 May 2026

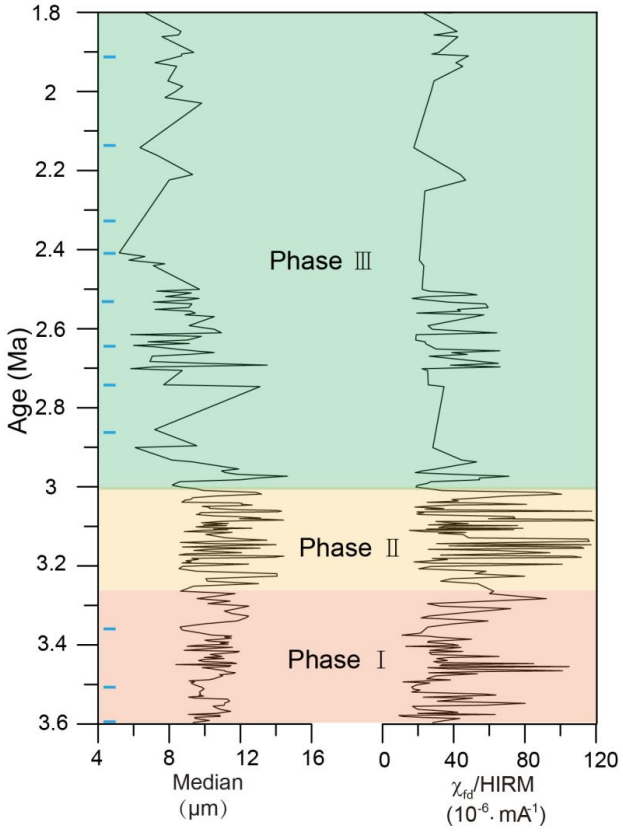

Figure 3. Variation trends of the χ_{fd}/HIRM and median grain size records during 3.6-1.8 Ma. The blue rectangles represent the halite layers.

Based on lithology and the variation patterns of the χ_{fd}/HIRM and median grain size records, the paleoclimatic sequence can be divided into three phases (Fig. 3). During 3.6-3.25 Ma (0-117 m; Phase I), χ_{fd}/HIRM values show large-amplitude fluctuations, ranging from 11.3×10^{-6} to 105×10^{-6} Am^{-1}, with an average of 37.6×10^{-6} Am^{-1} (Fig. 3). median grain size values range from 8.3 to 12.4 μm, with an average of 10.48 μm (Fig. 3). These two records display similar variation trends. In addition, the three thick halite layers observed in the stratigraphic sequence correspond well to

https://doi.org/10.5194/egusphere-2026-2580
Preprint. Discussion started: 13 May 2026

three low-value intervals in both the χ_{fd}/HIRM and median grain size records (Fig. 3). During 3.25-2.95 Ma (117-220 m; Phase II), the published χ_{fd}/HIRM record exhibits high-frequent fluctuations, with an average of 52.6×10^{-6} Am^{-1} (Fig. 3). The published median grain size record shows similar fluctuations, with an average of 11.2 μm (Fig. 3). No thick halite layers occur in the stratigraphic sequence during this interval (Fig. 3). During 2.95-1.8 Ma (220-453 m; Phase III), χ_{fd}/HIRM values range from 16.6×10^{-6} to 66×10^{-6} Am^{-1}, with an average of 36×10^{-6} Am^{-1} (Fig. 3). Median grain size values range from 5.1 to 13.5 μm, with an average of 8.36 μm (Fig. 3). Lithological observations indicate that halite layers occur more frequently during 2.95-1.8 Ma than during 3.6-3.25 Ma (Fig. 3).

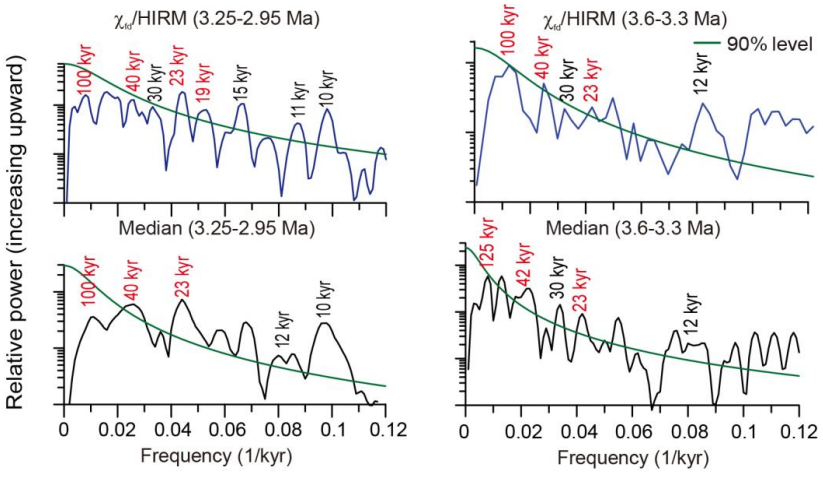

Figure 4. Results of spectral analyses of the reconstructed χ_{fd}/HIRM and median grain size records during 3.6-3.3 Ma and the published χ_{fd}/HIRM and median grain size records during 3.25-2.95 Ma. The orbital cycles revealed by these two paleoclimatic records during 3.6-3.3 Ma passed the 90% confidence level.

Our sampling yields an average resolution of ~4 kyr for the 3.6-3.3 Ma interval

https://doi.org/10.5194/egusphere-2026-2580
Preprint. Discussion started: 13 May 2026

(82 samples) and ~19 kyr for the 2.95-1.8 Ma interval (62 samples), indicating that the sampling resolution for the 3.6-3.3 Ma interval is sufficient to detect precession-, obliquity-, and eccentricity-scale cycles. Spectral analysis shows that the χ_{fd}/HIRM record is dominated by 100-kyr cycles, with relatively weak 40- and 23-kyr cycles, and the median grain size record is characterized mainly by 125-kyr cycles, together with weak 42- and 23-kyr cycles (Fig. 4). In addition, several non-orbital cycles, including 30-kyr and semiprecessional (~12-kyr) cycles, are also present and may reflect beats or harmonics of orbital cyclicities (Fig. 4).

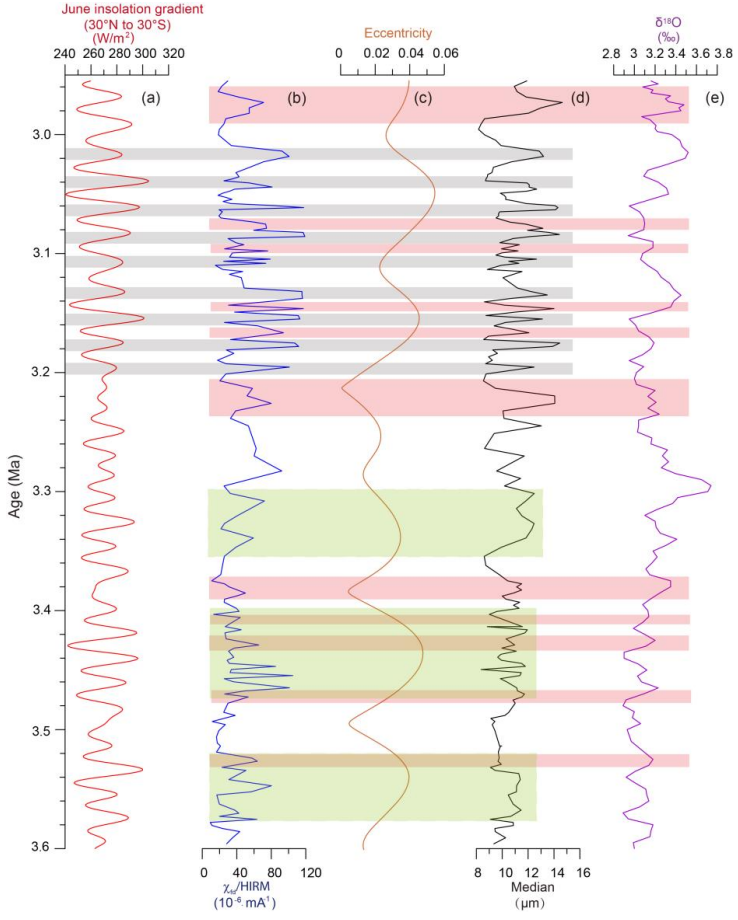

https://doi.org/10.5194/egusphere-2026-2580
Preprint. Discussion started: 13 May 2026

Figure 5. Comparison of the GS χ_{fd}/HIRM and median grain size records with insolation, eccentricity and benthic oxygen isotope stack during 3.6-2.95 Ma. (a) June insolation gradient (Laskar et al., 2004). (b) GS χ_{fd}/HIRM. (c) GS median grain size. (d) Eccentricity (Laskar et al., 2004) (e) Benthic $\delta^{18}O$ stack (Lisiecki and Raymo, 2005). The χ_{fd}/HIRM and median grain size data during 3.25-2.95 Ma have been published by Luo et al. (2024). The green, gray and pink bands emphasize the potential corresponding relationships between χ_{fd}/HIRM, median grain size, benthic $\delta^{18}O$ stack, eccentricity and insolation.

The dominant 100-kyr cyclicity in the χ_{fd}/HIRM and median grain size records during 3.6-3.3 Ma differs from the previously reported precession-dominated pattern during 3.25-2.95 Ma (Fig. 4). Comparison with eccentricity (Laskar et al., 2004) shows that high-eccentricity intervals correspond well to peak intervals in both records between 3.6 and 3.3 Ma (Fig. 5), consistent with dominant 100-kyr cyclicity during this interval. This interpretation is further supported by the similar phase relationship between eccentricity and both records at the 100-kyr band (Fig. 6a, e). In contrast, most high-insolation intervals shown by the June insolation gradient (30°N to 30°S) do not correspond to peak values in either record between 3.6 and 3.3 Ma, unlike the relationship observed during 3.25-2.95 Ma (Fig. 5). This mismatch, together with the weak 20-kyr signal (Fig. 6d, h), suggests that insolation did not directly force GS paleoclimatic variations during 3.6-3.3 Ma. In addition, five high-value intervals in the χ_{fd}/HIRM and median grain size records correspond well with those in the benthic oxygen isotope stack (Lisiecki and Raymo, 2005), similar to

https://doi.org/10.5194/egusphere-2026-2580
Preprint. Discussion started: 13 May 2026

the relationship observed during 3.25-2.95 Ma (Fig. 5). Both records also show a similar phase relationship with the benthic oxygen isotope stack at the 40-kyr band (Fig. 6b, f), but an inverse phase relationship with insolation at the same band (Fig. 6c, g), suggesting that ice sheets, rather than insolation, likely influenced the 40-kyr signal in the GS paleoclimatic records.

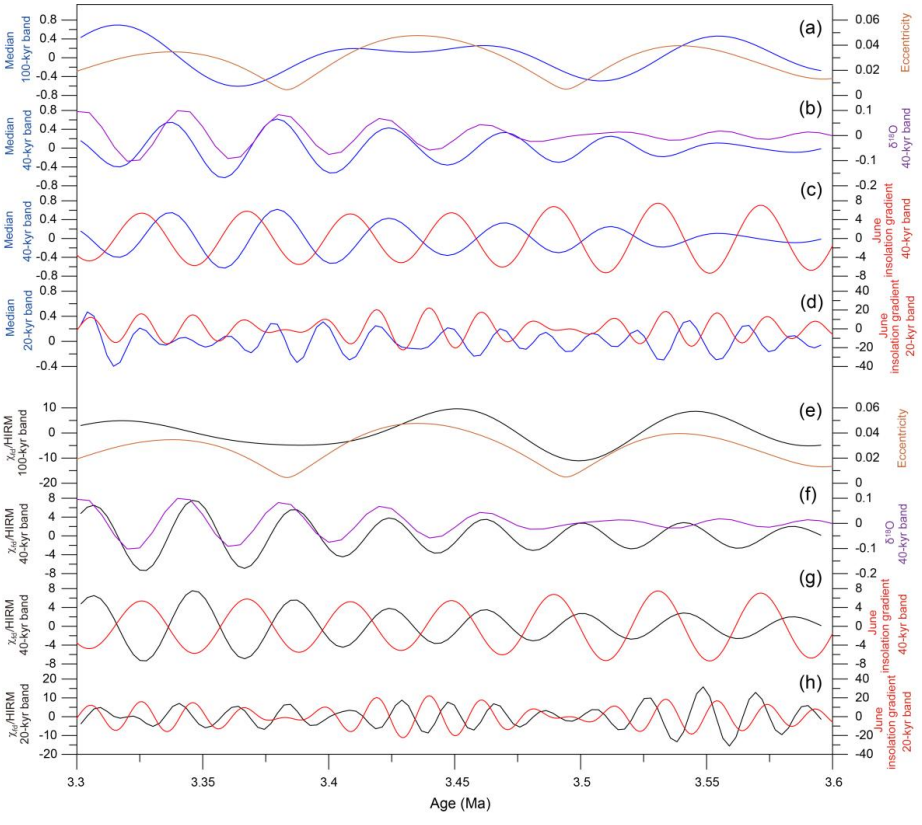

Figure 6. Comparison of the filtered χ_{fd}/HIRM and median grain size records from the GS section with the eccentricity, the filtered June insolation gradient and the filtered benthic oxygen isotope stack during 3.6-3.3 Ma. (a) and (e) χ_{fd}/HIRM and median grain size records at the 100-kyr band with eccentricity. (b) and (f) χ_{fd}/HIRM, median grain size and benthic $\delta^{18}O$ stack at the filtered 40-kyr band. (c) and (g)

https://doi.org/10.5194/egusphere-2026-2580
Preprint. Discussion started: 13 May 2026

χ_{fd}/HIRM, median grain size and June insolation gradient at the filtered 40-kyr band. (d) and (h) χ_{fd}/HIRM, median grain size and June insolation gradient at the filtered 20-kyr band. The 20-kyr central frequency = 0.05 kyr^{-1}, and the bandwidth = 0.012 kyr^{-1}. The 40-kyr central frequency = 0.024 kyr^{-1}, and the bandwidth = 0.004 kyr^{-1}. The 100-kyr central frequency = 0.01 kyr^{-1}, and the bandwidth = 0.002 kyr^{-1}.

5 Discussion

5.1 Late Pliocene-Quaternary precipitation variations in the western Qaidam Basin

The χ_{fd}/HIRM proxy has been shown to be sensitive to precipitation variations in arid to semiarid environments because χ_{fd} reflects pedogenic nanometer-scale ferrimagnetic grains, whereas HIRM mainly reflects hematite formed under relatively dry conditions (Luo et al., 2024). Therefore, their ratio records the relative balance between wetter and drier weathering conditions. Previous studies further indicate that this proxy can be applied in Qaidam fluvial-lacustrine sediments where magnetic minerals were not significantly dissolved after deposition (Nie et al., 2017; Su et al., 2019; Ren et al., 2020; Luo et al., 2024). The median grain size can also serve as an indirect precipitation proxy because coarser particles in closed and shallow lacustrine settings generally reflect stronger hydrodynamic conditions associated with increased runoff and precipitation (Su et al., 2019; Yang et al., 2020; Luo et al., 2024). In the GS section, the similar variation patterns of χ_{fd}/HIRM and median grain size during 3.6-3.25 Ma suggest that these two proxies consistently recorded precipitation variations.

https://doi.org/10.5194/egusphere-2026-2580
Preprint. Discussion started: 13 May 2026

The deposition of halite is generally associated with intensified aridity in arid regions (Song et al., 2013; Zhang et al., 2013; Gu et al., 2015; Luo et al., 2018). Therefore, the absence of halite layers likely reflects relatively wetter conditions during 3.25-2.95 Ma. This interpretation is consistent with paleoclimatic records from the HTG section in the western Qaidam Basin, which also indicate climatic wetting during the mPWP (Su et al., 2024). In addition, the χ_{fd}/HIRM and median grain size records reported here, together with the previously published GS records (Luo et al., 2024), show that precipitation during 3.25-2.95 Ma was higher than during 3.6-3.25 Ma and 2.95-1.8 Ma. Taken together, these observations suggest that the relatively wet climate recorded in the GS section during the mPWP was likely associated with enhanced precipitation under a strengthened EASM. Previously published records from the GS section further indicate that precipitation variations there were significantly influenced by the intensified EASM during the mPWP (Luo et al., 2024). A possible mechanism for this monsoon intensification is the intensification and westward extension of the western Pacific subtropical high (Huang et al., 2019). Climate model simulations suggest that enhanced land-sea thermal contrast between the East Asian continent and the equatorial western Pacific during the mPWP may have promoted the intensification and westward expansion of the western Pacific subtropical high, thereby enhancing the EASM (Huang et al., 2019). This inference may further imply that, under continued global warming, the Qaidam Basin could receive increased summer moisture, potentially associated with a westward extension of the western Pacific subtropical high that favors a northwestward shift in EASM

https://doi.org/10.5194/egusphere-2026-2580
Preprint. Discussion started: 13 May 2026

311 precipitation.

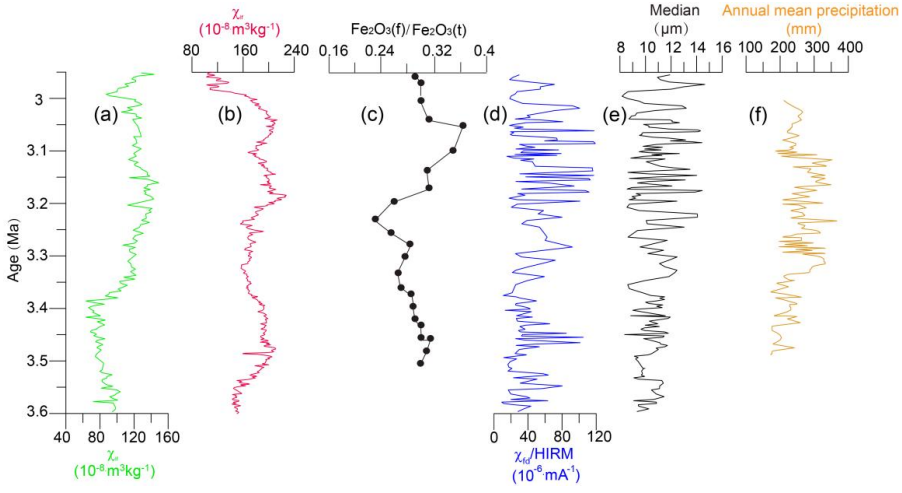

312

313 **Figure 7.** Comparison of the GS χ_{fd}/HIRM and median grain size records with the
314 paleoclimatic records affected by the EASM precipitation during 3.6-2.95 Ma. (a)
315 Magnetic susceptibility at low frequency (χ_{lf}) from the Chaona section (Song et al.,
316 2001). (b) Magnetic susceptibility at low frequency (χ_{lf}) from the Shilou section (Ao
317 et al., 2016). (c) The ratio of free iron (Fe_2O_3(f)) to total iron (Fe_2O_3(t)) content of the
318 Pianguan section (Yang et al., 2018). (d) GS χ_{fd}/HIRM. (e) GS median grain size. (f)
319 Annual mean precipitation variations based on the pollen records from the SG-1b core
320 (Schwarz et al., 2022).

321 The precipitation variations in the GS section during 3.6-2.95 Ma are similar to
322 those recorded in the Chinese Loess Plateau and the SG-1b core from the western
323 Qaidam Basin, both of which were influenced by the EASM (Fig. 7). This similarity
324 suggests that EASM-related summer moisture likely also reached the GS section, at
325 least during 3.6-3.25 Ma. From 2.95-1.8 Ma, however, the low sampling resolution of
326 the precipitation records precludes identification of clear temporal trends (Fig. 3) and

https://doi.org/10.5194/egusphere-2026-2580
Preprint. Discussion started: 13 May 2026

prevents detailed comparison with precipitation records from the monsoon region. Nevertheless, the more frequent occurrence of halite layers suggests intensified aridification during 2.95-1.8 Ma (Fig. 3). This result is supported by other paleoenvironmental records from the western Qaidam Basin. For example, pollen records from the SG-3 core suggest that the Qaidam Basin was a drier environment no later than ~3 Ma (Miao et al., 2013). The oxygen isotope records from the HTG section indicate that the Qaidam Basin has been characterized by a drier climate since 2.9 Ma (Su et al., 2024). Taken together, these observations suggest enhanced aridification in the western Qaidam Basin following the Late Pliocene warmth.

5.2 Nonlinear response of precipitation to insolation forcing during 3.6-3.3 Ma

The published precipitation records of the GS section reveal that precipitation in the Qaidam Basin was dominated by the 20-kyr precession cyclicity during the mPWP, and suggest that the June insolation gradient (30°N minus 30°S) directly forced precipitation variations in the Qaidam Basin during this interval (Luo et al., 2024). In contrast, the reconstructed precipitation records of the GS section reveal that precipitation in the Qaidam Basin was dominated by the 100-kyr eccentricity cyclicity during 3.6-3.3 Ma. It is widely believed that the insolation variations associated with the eccentricity signal of the Earth are much weaker than those associated with the precession and obliquity signals, although eccentricity can affect the insolation variations through the modulation of precession (Luo et al., 2018; Wang et al., 2023). Thus, our precipitation records may show a nonlinear response to the insolation variations during 3.6-3.3 Ma. This finding is in line with the magnetic susceptibility

https://doi.org/10.5194/egusphere-2026-2580
Preprint. Discussion started: 13 May 2026

records from the YZ01 borehole in the Xinding Basin, Shanxi Graben, North China, revealing that precipitation was dominated by the 100-kyr eccentricity cyclicity before 3.3 Ma, and constituted a nonlinear response to insolation (Wang et al., 2023). Moreover, a similar nonlinear response to insolation was found in the Rb/Sr records from the Huangdigou section in the Sanmenxia Basin, North China (Zhang et al., 2022). In the Qaidam Basin, the pollen records from the SG-1b core reveal that there was a strong link between the 100-kyr cyclicity in the precipitation records and the eccentricity forcing during 3.5-3.0 Ma (Schwarz et al., 2022).

Interestingly, precipitation was stronger during intervals dominated by a 20-kyr precessional signal, whereas it was relatively weaker during intervals characterized mainly by a 100-kyr eccentricity signal. However, this contrast does not simply reflect differences in precipitation intensity itself. Rather, it suggests that the dominant processes controlling the westward penetration of summer moisture into the western Qaidam Basin varied under different climatic background states. During the wetter interval of 3.25-2.95 Ma, EASM-related moisture could penetrate farther inland, allowing precipitation to respond more directly to insolation forcing. By contrast, during 3.6-3.3 Ma, when precipitation was weaker, the dominant 100-kyr cyclicity suggests a more indirect control on summer moisture delivery, likely involving changes in large-scale boundary conditions. This indirect control may reflect several mechanisms through which eccentricity-scale forcing influenced precipitation in the GS section during 3.6-3.3 Ma. First, the dominant 100-kyr cyclicity can be interpreted as linked to insolation-driven Antarctic ice sheet forcing of the monsoonal intensity.

https://doi.org/10.5194/egusphere-2026-2580
Preprint. Discussion started: 13 May 2026

That is, eccentricity controls Antarctic ice sheets in a nonlinear way, thereby affecting the expansion and contraction of Antarctic ice sheets and hence controlling the EASM intensity through the modulation of the thermal contrast between Eurasia and the surrounding oceans or the increase in Pacific and Atlantic meridional overturning circulation (Zhang et al., 2022; Wang et al., 2023). Because the Arctic ice sheets did not develop on a large scale before ~2.7 Ma (Brigham-Grette et al., 2013; Rahaman et al., 2020; Bridges et al., 2023), the benthic oxygen isotope stack mainly represented Antarctic ice sheet variations. Thus, at the 100-kyr band, the comparison of these two precipitation records in the GS section with the eccentricity and benthic oxygen isotope stack seems to support this hypothesis (Fig. 8). Second, the dominant 100-kyr cyclicity in the precipitation records could have been controlled by annual insolation instead of summer insolation. Because the annual insolation integrates seasonable insolation variations caused by precession, it has more power in eccentricity bands and weak power in precession bands (Lasker et al., 2004). However, more investigations are needed to validate this hypothesis.

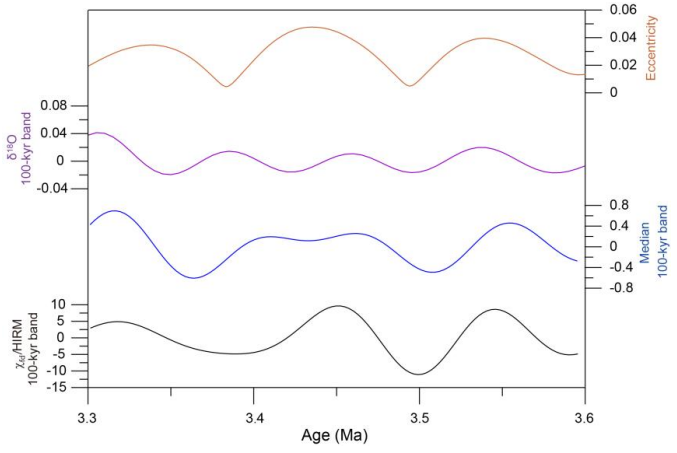

https://doi.org/10.5194/egusphere-2026-2580
Preprint. Discussion started: 13 May 2026

Figure 8. Comparison of the χ_{fd}/HIRM and median grain size records with the eccentricity and benthic oxygen isotope stack data. The χ_{fd}/HIRM, median grain size and benthic oxygen isotope stack data were filtered at the 100-kyr band.

Additionally, at the 40-kyr band, our precipitation records show a similar phase relationship with the benthic oxygen isotope stack, suggesting that Antarctic ice-sheet variability may have directly influenced precipitation in the Qaidam Basin during 3.6-3.3 Ma, rather than acting only indirectly through insolation-related forcing. This inference is consistent with the published GS precipitation records for 3.25-2.95 Ma (Luo et al., 2024), and together these results suggest that Antarctic ice-sheet variability directly modulated precipitation in the Qaidam Basin during the Late Pliocene.

6 Conclusions

Integrated χ_{fd}/HIRM and median grain size records from the GS section provide a continuous reconstruction of precipitation variability in the western Qaidam Basin during 3.6-1.8 Ma. The combined record shows that precipitation during 3.25-2.95 Ma was higher than during 3.6-3.25 Ma and 2.95-1.8 Ma, supporting the interpretation of relatively wetter conditions in the western Qaidam Basin during the mPWP. Comparison with previously published regional precipitation records further suggests that EASM-related summer moisture continued to reach the western Qaidam Basin during 3.6-3.25 Ma, although the associated precipitation was weaker than that during 3.25-2.95 Ma.

At the orbital timescale, precipitation variations during 3.6-3.3 Ma was

https://doi.org/10.5194/egusphere-2026-2580
Preprint. Discussion started: 13 May 2026

characterized mainly by 100-kyr cyclicity, in contrast to the previously reported precession-dominated pattern during 3.25-2.95 Ma. This shift indicates that the precession-dominated pattern was not persistent throughout the Late Pliocene in the western Qaidam Basin. Instead, the dominant periodicity of precipitation changed through time, implying that the processes controlling the westward penetration of summer moisture into the basin varied under different climatic background states. In particular, the stronger ~20-kyr signal during 3.25-2.95 Ma likely reflects a more direct response of precipitation to precessional insolation forcing under wetter conditions, whereas the dominant 100-kyr cyclicity during 3.6-3.3 Ma suggests a more indirect forcing response under relatively drier conditions. In addition, the phase relationship between the precipitation proxies and the benthic oxygen isotope stack at the 40-kyr band suggests that Antarctic ice-sheet variability may also have modulated hydroclimatic variability in the basin. Overall, these findings highlight that Late Pliocene precipitation variability in the western Qaidam Basin was shaped not only by changes in moisture availability, but also by shifts in the dominant climatic processes governing inland penetration of EASM-related summer moisture.

Data availability

All data for this paper are available upon request.

Author contributions

All authors approved the manuscript and agreed on its submission. **ZL:** writing-original draft, methodology, conceptualization, formal analysis, data collection, funding acquisition, investigation, resources. **HW:** Writing-review &

https://doi.org/10.5194/egusphere-2026-2580
Preprint. Discussion started: 13 May 2026

editing, investigation, data collection. **XY:** Writing-review & editing, investigation. **ZZ, ZS, JY and WC:** investigation, sample processing. **QS:** investigation, sample processing, funding acquisition. **YL and SH:** investigation.

Competing interests

The authors declare that they have no conflict of interest.

Acknowledgments

This work was financially supported by the National Natural Science Foundation of China (grants 42202215, 42302213 and 42401004), the Key Foundation of the Education Department of Hunan Province (21A0424), the PhD Research Startup Foundation of Hunan University of Arts and Science (grants 23BSQD05, 23BSQD05), the Fund of Geography Subject ([2022]351) and the Open Foundation of MOE Key Laboratory of Western China's Environmental System, Lanzhou University and the Fundamental Research Funds for the Central Universities (lzujbky-2021-kb01).

References

Ao, H., Roberts, A.P., Dekkers, M.J., Liu, X., Rohling, E.J., Shi, Z., An, Z., and Zhao, X.: Late Miocene-Pliocene Asian monsoon intensification linked to Antarctic ice-sheet growth, Earth Planet. Sci. Lett., 444, 75-87, doi:https://doi.org/10.1016/j.epsl.2016.03.028, 2016.

Bartoli, G., Honisch, B., and Zeebe, R.E.: Atmospheric CO_2 decline during the Pliocene intensification of Northern Hemisphere glaciations, Paleoceanography, 26, PA4213, doi:https://doi.org/10.1029/2010pa002055, 2011.

Badger, M. P. S., Schmidt, D. N., Mackensen, A., and Pancost, R. D.: High resolution alkenone palaeobarometry indicates relatively stable pCO2 during the Pliocene

https://doi.org/10.5194/egusphere-2026-2580
Preprint. Discussion started: 13 May 2026

(3.3 to 2.8 Ma), Philos. Trans. A Math. Phys. Eng. Sci., 371, 20130094, doi:https://doi.org/10.1098/rsta.2013.0094, 2013.

Bridges, J.D., Tarduno, J.A., Cottrell, R.D., and Herbert, T.D.: Rapid strengthening of westerlies accompanied intensification of Northern Hemisphere glaciation, Nat. Commun., 14, 3905, doi:https://doi.org/10.1038/s41467-023-39557-4, 2023.

Brigham-Grette, J., Melles, M., Minyuk, P., Andreev, A., Tarasov, P., DeConto, R., Koenig, S., Nowaczyk, N., Wennrich, V., and Rosén, P.: Pliocene warmth, polar amplification, and stepped Pleistocene cooling recorded in NE Arctic Russia, Science, 340(6139), 1421-1427, doi:https://doi.org/10.1126/science.1233137, 2013.

Bush, M., Horton, B.K., Saylor, J.E., and Nie, J.S.: Growth of the Qaidam Basin during Cenozoic exhumation in the northern Tibetan Plateau: Inferences from depositional patterns and multiproxy detrital provenance signatures, Lithosphere, 8(1), 58-82,doi:https://doi.org/10.1130/L449.1, 2016.

Burke, K.D., Williams, J.W., Chandler, M.A., Haywood, A.M., Lunt, D.J., and Ottobliesner, B.L.: Pliocene and Eocene provide best analogs for near-future climates, Proc. Natl. Acad. Sci., 115(52), 13288-13293, doi:https://doi.org/10.1073/pnas.1809600115, 2018.

Cai, M.T., Fang, X.M., Wu, F.L., Miao, Y.F., and Appel, E.: Pliocene-Pleistocene stepwise drying of Central Asia: Evidence from paleomagnetism and sporopollen record of the deep borehole SG-3 in the western Qaidam Basin, NE Tibetan Plateau, Glob. Planet. Chang., 94-95, 72-81, https://doi.org/10.1016/j.gloplacha.2012.07.002, 2012.

Dowsett, H.J., Robinson, M.M., Haywood, A.M., Salzmann, U., Hill, D.J., Sohl, L.E., Chandler, M., Williams, M., Foley, K., and Stoll, D.K.: The PRISM3D

https://doi.org/10.5194/egusphere-2026-2580
Preprint. Discussion started: 13 May 2026

paleoenvironmental reconstruction, Stratigraphy, 7, https://doi.org/10.1111/j.1475-4983.2010.00949.x, 2010.

Gu, N., Jiang, W.Y., Wang, L., Zhang, E.L., Yang, S.L., and Xiong, S.F.: Rainfall thresholds for the precipitation of carbonate and evaporite minerals in modern lakes in northern China, Geophys. Res. Lett., 42 (14), 5895-5901, https://doi.org/10.1002/2015GL064340, 2015.

Haywood, A.M., Ridgwell, A., Lunt, D.J., Hill, D.J., Pound, D.J., and Dowsett, H.J.: Are there pre-Quaternary geological analogues for a future greenhouse warming? Philos. T. R. Soc. A, 369 (1938), 933-956, https://doi.org/10.1098/rsta.2010.0317, 2011.

Haywood, A., Dowsett, H., and Dolan, A.: Integrating geological archives and climate models for the mid-Pliocene warm period, Nat. Commun., 7, 10646, https://doi.org/10.1038/ncomms10646, 2016.

Hearty, P. J., Rovere, A., Sandstrom, M.R., O'Leary, M. J., Roberts, D., and Raymo, M. E.: Pliocene-Pleistocene stratigraphy and sea-level estimates, Republic of South Africa with implications for a 400 ppmv CO_2 world, Paleoceanogr. Paleoclimatol., 35, e2019PA003835, https://doi.org/10.1029/2019PA003835, 2020.

Herbert, T.D., Lawrence, K.T., Tzanova, A., Peterson, L.C., Caballero-Gill, R., and Kelly, C.S.: Late Miocene global cooling and the rise of modern ecosystems, Nat. Geosci., 9(11), 843-847, https://doi.org/10.1038/ngeo2813, 2016.

Huang, X.F., Jiang, D.B., Dong, X.X., Yang, S.L., Su, B.H., Li, X.Y., Tang, Z.H., and Wang, Y.D.: Northwestward Migration of the Northern Edge of the East Asian Summer Monsoon During the Mid-Pliocene Warm Period: Simulations and

https://doi.org/10.5194/egusphere-2026-2580
Preprint. Discussion started: 13 May 2026

503 Reconstructions, J. Geophys. Res., 124, 1392-1404,
504 https://doi.org/10.1029/2018jd028995, 2019.
505 Huang, X.F., Yang, S.L., Haywood, A., Jiang, D.B., Wang, Y.D., Sun, M.M., Tang,
506 Z.H., and Ding, Z.L.: Warming-induced northwestward migration of the Asian
507 summer monsoon in the geological past: Evidence from climate simulations and
508 geological reconstructions, J. Geophys. Res-Atmos., 126, e2021JD035190,
509 https://doi.org/10.1029/2021JD035190, 2021.
510 Koutsodendris, A., Allstadt, F.J., Kern, O.A., Kousis, I., Schwarz, F., Vannacci, M.,
511 Woutersen, A., Appel, E., Berke, M.A., and Fang, X. M.: Late Pliocene
512 vegetation turnover on the NE Tibetan Plateau (Central Asia) triggered by early
513 Northern Hemisphere glaciation, Glob. Planet. Chang., 180, 117-125,
514 https://doi.org/10.1016/j.gloplacha.2019.06.001, 2019.
515 Laskar, J., Robutel, P., Joutel, F., Gastineau, M., Correia, A.C.M., and Levrard, B.: A
516 long-term numerical solution for the insolation quantities of the Earth, Astron.
517 Astrophys., 428, 261-285, https://doi.org/10.1051/0004-6361:20041335, 2004.
518 Li, M.H., Fang, X.M., Yi, C.L., Gao, S.P., Zhang, W.L., and Galy, A.: Evaporite
519 minerals and geochemistry of the upper 400 m sediments in a core from the
520 Western Qaidam Basin, Tibet, Quatern. Int., 218(1-2), 176-189,
521 https://doi.org/10.1016/j.quaint.2009.12.013, 2010.
522 Lisiecki, L.E., and Raymo, M.E.: A Plio-Pleistocene stack of 57 globally distributed
523 benthic $\delta^{18}O$ records, Paleoceanography, 20, PA1003,
524 https://doi.org/10.1029/2004pa001071, 2005.
525 Lunt, D.J., Haywood, A.M., Schmidt, G.A., Salzmann, U., Dowsett, H.J., and Loptson,
526 C.A.: On the causes of mid-Pliocene warmth and polar amplification, Earth

https://doi.org/10.5194/egusphere-2026-2580
Preprint. Discussion started: 13 May 2026

Planet. Sci. Lett., 321-322, 128-138, https://doi.org/10.1016/j.epsl.2011.12.042, 2012.

Luo, Z., Su, Q.D., Wang, Z., Heermance, R.V., Garzione, C.N., Li, M., Ren, X.P., Song, Y.G., and Nie, J.S.: Orbital forcing of Plio-Pleistocene climate variation in a Qaidam Basin lake based on paleomagnetic and evaporite mineralogic analysis, Palaeogeogr. Palaeoclimatol. Palaeoecol., 510, 31-39, https://doi.org/10.1016/j.palaeo.2017.09.022, 2018.

Luo, Z., Nie, J.S., Moe, A.E., Heermance, R.V., Garzione, C; Herbert, T.D., Wang, Z., Li, H., Zhang. R., Zhao, X.M., and Salzmann, U.: Joint insolation and ice sheet/CO2 forcing on northern China precipitation during Pliocene warmth, Sci. Bull., 66(4), 319-322, https://doi.org/10.1016/j.scib.2020.10.025, 2021.

Luo, Z., Wang, H.S., Heermance, R.V., Nie, J.S., Yang, J., Yu, X.L., Wang, Z., Zhang, Z., and Su, Q.D.: June insolation gradient and ice sheet forcing on Qaidam precipitation during the middle Piacenzian warm period, Palaeogeogr. Palaeoclimatol. Palaeoecol., 648, 112277, https://doi.org/10.1016/j.palaeo.2024.112277, 2024.

Miao, Y.F., Fang, X.M., Wu, F.L., Cai, M.T., Song, C.H., Meng, Q.Q., and Xu, L.: Late Cenozoic continuous aridification in the western Qaidam Basin: evidence from sporopollen records, Clim. Past, 9(4), 1863-1877, https://doi.org/10.5194/cp-9-1863-2013, 2013.

Nie, J.S., Garzione, C.N., Su, Q.D., Liu, Q.S., Zhang, R., Heslop, D., Necula, C., Zhang, S.H., Song, Y.G., and Luo, Z.: Dominant 100,000-year precipitation cyclicity in a late Miocene lake from Northeast Tibet, Sci. Adv., 3(3), e1600762, https://doi.org/10.1126/sciadv.1600762, 2017.

https://doi.org/10.5194/egusphere-2026-2580
Preprint. Discussion started: 13 May 2026

551 Raymo, M.E., Lisiecki, L.E., and Nisancioglu, K.H.: Plio-Pleistocene ice volume,
552 Antarctic climate, and the global $\delta^{18}O$ record, Science, 313, 492-495,
553 https://doi.org/10.1126/SCIENCE.1123296, 2006.
554 Ravelo, A.C., Andreasen, D.H., Lyle, M., Olivarez, L.A., and Wara, M.W.: Regional
555 climate shifts caused by gradual global cooling in the Pliocene epoch, Nature,
556 429, 263-267, https://doi.org/10.1038/nature02567, 2004.
557 Rahaman, W., Smik, L., Köseoğlu, D., N, L., Tarique, M., Thamban, M., Haywood,
558 A., Belt, S.T., and Knies, J.: Reduced Arctic sea ice extent during the
559 mid-Pliocene Warm Period concurrent with increased Atlantic-climate regime,
560 Earth Planet. Sci. Lett., 550, 116535, https://doi.org/10.1016/j.epsl.2020.116535,
561 2020.
562 Ren, X.P., Nie, J.S., Saylor, J.E., Wang, X.X., Liu, F.B., and Horton, B.K.:
563 Temperature control on silicate weathering intensity and evolution of the
564 Neogene East Asian summer monsoon, Geophys. Res. Lett., 47(15),
565 e2020GL088808, https://doi.org/10.1029/2020gl088808, 2020.
566 Reguero, M.A., Candela, A.M., and Alonso, R.N.: Biochronology and biostratigraphy
567 of the Uquía Formation (Pliocene-early Pleistocene, NW Argentina) and its
568 significance in the Great American Biotic Interchange, J. S. Am. Earth Sci.,
569 23(1), 1-16, https://doi.org/10.1016/j.jsames.2006.09.005, 2007.
570 Salzmann, U., Haywood, A. M., Lunt, D. J., Valdes, P. J., and Hill, D. J.: A new
571 global biome reconstruction and data-model comparison for the Middle Pliocene,
572 Global Ecol. Biogeogr., 17, 432-447,
573 https://doi.org/10.1111/j.1466-8238.2008.00381.x, 2008.
574 Salzmann, U., Williams, M., Haywood, A.M., Johnson, A.L.A., Kender, S., and
575 Zalasiewicz, J.: Climate and environment of a Pliocene warm world, Palaeogeogr.

https://doi.org/10.5194/egusphere-2026-2580
Preprint. Discussion started: 13 May 2026

Palaeoclimatol. Palaeoecol., 309(1-2), 1-8, https://doi.org/10.1016/j.palaeo.2011.05.044, 2011.

Schwarz, F., Salzmann, U., Koutsodendris, A., Nie, J.S., Friedrich, O., Ni, J., Garzione, C., Fang, X.M., Wu, F.L., Woodward, J., Appel, E., and Prosset, J.: Controls of precipitation and vegetation variability on the NE Tibetan Plateau during the Late Pliocene warmth (~3.5-3.0 Ma), Glob. Planet. Chang., 208, 103707, https://doi.org/10.1016/j.gloplacha.2021.103707, 2022.

Song, C.H., Hu, S.H., Han, W.X., Zhang, T., Fang, X.M., Gao, J.P., and Wu, F.L.: Middle Miocene to earliest Pliocene sedimentological and geochemical records of climate change in the western Qaidam Basin on the NE Tibetan Plateau, Palaeogeogr. Palaeoclimatol. Palaeoecol., 395(2), 67-76, https://doi.org/10.1016/j.palaeo.2013.12.022, 2013.

Song, Y.G., Fang, X.M., Li, J.J., An, Z.S., and Miao, X.D.: The Late Cenozoic uplift of the Liupan Shan, China, Sci. China Ser. D-Earth Sci., 44, 176-184, https://doi.org/10.1007/bf02911985, 2001.

Su, Q.D., Nie, J.S., Meng, Q.Q., Heermance, R., Gong, L.S., Luo, Z., Wang, Z., Zhang, R., and Garzione, C.: Central Asian Drying at 3.3 Ma Linked to Tropical Forcing? Geophys. Res. Lett., 46(17-18), 10561-10567, https://doi.org/10.1029/2019GL084648, 2019.

Su, Q.D., Nie, J.S., Han, W.X., Garzione, C.N., and Gao, P.: Obliquity forcing of Late Pliocene–Early Pleistocene aridification in the Qaidam Basin, NE Tibetan Plateau, Palaeogeogr. Palaeoclimatol. Palaeoecol., 635, 111951, https://doi.org/10.1016/j.palaeo.2023.111951, 2024.

Vieira, M., Pound, M.J., and Pereira, D.I.: The Late Pliocene palaeoenvironments and palaeoclimates of the western Iberian Atlantic margin from the Rio Maior flora,

https://doi.org/10.5194/egusphere-2026-2580
Preprint. Discussion started: 13 May 2026

601 Palaeogeogr. Palaeoclimatol. Palaeoecol., 495, 245-258,
602 https://doi.org/10.1016/j.palaeo.2018.01.018, 2018.
603 Wan, S.M., Tian, J., Steinke, S., Li, A.C., and Li, T.G.: Evolution and variability of
604 the East Asian summer monsoon during the Pliocene: Evidence from clay
605 mineral records of the South China Sea, Palaeogeogr. Palaeoclimatol.
606 Palaeoecol., 293 (1-2), 237-247, https://doi.org/10.1016/j.palaeo.2010.05.025,
607 2010.
608 Wang, J.Y., Fang, X.M., Appel, E., and Zhang, W.L.: Magnetostratigraphic and
609 radiometric constraints on salt formation in the Qaidam Basin, NE Tibetan
610 Plateau, Quat. Sci. Rev., 78(11), 53-64,
611 https://doi.org/10.1016/j.quascirev.2013.07.017, 2013.
612 Wang, Z.X., Mao, Y.D., Zhang, R., Kemp, D. B., and Huang, C.J.: Links between
613 orbital forcing, Antarctic ice volume, and the East Asian hydrological cycle over
614 the Pliocene, J. Geophys. Res. Atmos., 128, e2023JD039519,
615 https://doi.org/10.1029/2023jd039519, 2023.
616 Wehausen, R., and Brumsack, H.J.: Astronomical forcing of the East Asian monsoon
617 mirrored by the composition of Pliocene South China Sea sediments, Earth
618 Planet. Sci. Lett., 201, 621-636,
619 https://doi.org/10.1016/S0012-821X(02)00746-X, 2002.
620 Yang, S.L., Ding, Z.L., Feng, S.H., Jiang, W.Y., Huang, X.F., and Guo, L.C.: A
621 strengthened East Asian Summer Monsoon during Pliocene warmth: Evidence
622 from 'red clay' sediments at Pianguan, northern China, J. Asian Earth Sci., 155,
623 124-133, https://doi.org/10.1016/j.jseaes.2017.10.020, 2018.
624 Yang, L.Y., Zhang, W.L., Fang, X.M., Cai, M.T., and Lu, Y.: Aridification recorded
625 by lithofacies and grain size in a continuous Pliocene-Quaternary lacustrine

https://doi.org/10.5194/egusphere-2026-2580
Preprint. Discussion started: 13 May 2026

626 sediment record in the western Qaidam Basin, NE Tibetan Plateau, Palaeogeogr.
627 Palaeoclimatol. Palaeoecol., 556, 109903,
628 https://doi.org/10.1016/j.palaeo.2020.109903, 2020.
629 Zhang, Z.G., Han, W.X., Fang, X.M., Song, C.H., and Li, X.Y.: Late
630 Miocene–Pleistocene aridification of Asian inland revealed by geochemical
631 records of lacustrine-fan delta sediments from the western Tarim Basin, NW
632 China, Palaeogeogr. Palaeoclimatol. Palaeoecol., 377(2), 52-61,
633 https://doi.org/10.1016/j.palaeo.2013.03.008, 2013.
634 Zhang, Z., Licht, A., De Vleeschouwer, D.D., Wang, Z.X., Li, Y.Z., Kemp, D. B.,
635 Tan, L.C., Zhang, R., Qaing, X.K., and Huang, C.J.: East Asian monsoonal
636 climate sensitivity changed in the Late Pliocene in response to Northern
637 Hemisphere glaciations, Geophys. Res. Lett., 49,
638 e2022GL101280,https://doi.org/10.1029/2022gl101280, 2022.
639 Zhou, X.Q., and Liu, C.L.: Mid-Piacenzian and future changes in South Asian
640 precipitation under global warming, Glob. Planet. Chang., 248, 104760,
641 https://doi.org/10.1016/j.gloplacha.2025.104760, 2025.